Deformation band development as a function of intrinsic host-rock properties in Triassic Sherwood Sandstone

JOSHUA GRIFFITHS[1]*, DANIEL R. FAULKNER[1], ALEXANDER P. EDWARDS[2] & RICHARD H. WORDEN[1]

[1]*School of Earth, Ocean and Ecological Sciences, University of Liverpool, Liverpool L69 3GP, UK*

[2]*Ikon Science, Teddington, Middlesex TW11 0JR, UK*

**Corresponding author (e-mail: j.griffiths1@liverpool.ac.uk)*

Abstract: Deformation bands significantly alter the local petrophysical properties of sandstone reservoirs, although it is not known how the intrinsically variable characteristics of sandstones (e.g. grain size, sorting and mineralogy) influence the nature and distribution of deformation bands. To address this, cataclastic deformation bands within fine- and coarse-grained Triassic Sherwood Sandstone at Thurstaston, UK were analysed, for the first time, using a suite of petrographical techniques, outcrop studies, helium porosimetry and image analysis. Deformation bands are more abundant in the coarse-grained sandstone than in the underlying fine-grained sandstone. North- and south-dipping conjugate sets of cataclastic bands in the coarse-grained sandstone broadly increase in density (defined by number/m^2) when approaching faults. Microstructural analysis revealed that primary grain size controls deformation band density. Deformation bands in both coarse and fine sandstones led to significantly reduced porosity, and so can represent barriers or baffles to lateral fluid flow. Microstructural data show preferential cataclasis of K-feldspar grains within the host rock and deformation band. The study is of direct relevance to the prediction of reservoir quality in several petroleum-bearing Lower Triassic reservoirs in the near offshore, as deformation band development occurred prior to Carboniferous source-rock maturation and petroleum migration.

The oil and gas industry has expressed a growing interest in deformation bands because they are subseismic, tabular zones of strain localization that can cause large changes to a reservoir's petrophysical properties (Ballas *et al.* 2013). Examples of permeability alteration include the Clair Field, west of Shetland, UK, where deformation bands provide a conduit to lateral fluid flow during the early stages of deformation band formation that initially increased porosity (Baron *et al.* 2008). At the Anschutz Ranch East Field, Wyoming, USA, deformation bands separate clean sandstones and bitumen-stained sandstones, implying a strong impact on oil and gas movement (Solum *et al.* 2010). At the Arroyo Grande Field, California, USA, steam conductivity parallel to deformation bands is reported to be nine times higher than conductivity perpendicular to deformation bands, with tar deposits present on only one side of the deformation bands (Solum *et al.* 2010). Data presented in this study could potentially maximize near-term production targets in the Morecambe, Hamilton, Douglas and Lennox oil and gas fields within the neighbouring East Irish Sea Basin.

Millimetres to centimetres in width, with lengths of several metres or more (Schultz & Soliva 2012), deformation bands have been kinematically classified as one of three end members, namely: dilation bands (pore volume increase); shear bands (pore volume increase, decrease or no change); or compaction bands (pore volume decrease) (Aydin *et al.* 2006; Torabi 2014). Deformation bands in this study will be classified by the predominant deformation mechanism: disaggregation; phyllosilicate smear; cataclasis; and solution and cementation (Fossen *et al.* 2007).

Disaggregation bands form due to shear-induced disaggregation of grains by grain rolling, grain-boundary sliding and the breakage of cements bonding grains, but show little or no evidence of grain crushing (Schultz *et al.* 2010). Phyllosilicate bands form in sandstones which contain >10–15% platy minerals, and 'deformation bands with clay smearing' form in sandstones which have a clay content >40% (Fisher & Knipe 2001; Cerveny *et al.* 2004; Fossen *et al.* 2007). Mechanical grain fracturing is the dominant process in cataclastic bands, where compaction and reorganization of broken

From: Armitage, P. J., Butcher, A. R., Churchill, J. M., Csoma, A. E., Hollis, C., Lander, R. H., Omma, J. E. & Worden, R. H. (eds) *Reservoir Quality of Clastic and Carbonate Rocks: Analysis, Modelling and Prediction.* Geological Society, London, Special Publications, **435**, http://doi.org/10.1144/SP435.11

grains significantly reduces porosity (Cerveny *et al.* 2004; Fossen 2010). Solution bands are produced when chemical compaction, or pressure solution, is the dominant process; they commonly form at shallow depths and contain minimal cataclasis (Fossen *et al.* 2007). Fresh mineral surfaces exposed by grain-boundary sliding and/or grain crushing provide preferential sites for cementation, thus creating cementation bands (Fossen *et al.* 2007).

The primary aim of this paper is to establish how intrinsic host-rock properties (grain size, grain size distribution, porosity and mineralogy) control the nature and distribution of deformation bands. Using a range of petrographical techniques, image analysing software and field techniques, this paper will address the following specific questions, using examples of deformation bands for the first time from Thurstaston, Wirral, UK (Lower Triassic Sherwood Sandstone Group):

- What types of deformation band are present at Thurstaston?
- What is the spatial relationship between deformation band density and fault proximity?
- What is the relationship between the nature of deformation bands and the instrinsic host-rock properties?
- What is the potential impact of the presence of deformation bands in nearby reservoirs in the same lithology?

Geological setting

Early Permian rifting formed a predominantly north–south-orientated asymmetrical half-graben, deepening towards the east (Mikkelsen & Floodpage 1997). The Cheshire Basin (Fig. 1a) formed in the hanging wall of the Wem–Red Rock Fault (Knott 1994; Beach *et al.* 1997; Mikkelsen & Floodpage 1997), a northerly continuation of the Permo-Triassic rift system (Rowe & Burley 1997) that extended from the Wessex Basin to the Scottish Inner Hebrides. Thermal subsidence prolonged rifting until the mid-Triassic, with normal faulting during the early Triassic and Jurassic modifying the basin morphology. Tertiary contraction generated uplift of up to 1500 m (Knott 1994; Beach *et al.* 1997; Ware & Turner 2002), with intra-Triassic uplift resulting in 700–900 m of erosion (Mikkelsen & Floodpage 1997; Rowley & White 1998; Ware & Turner 2002).

Potential organic-rich Carboniferous source-rock sediments (Mikkelsen & Floodpage 1997) in the Cheshire Basin are overlain unconformably by the Permian Collyhurst Sandstone, Manchester Marl and the Kinnerton Sandstone (Rowe & Burley 1997). The Sherwood Sandstone Group (the focus of this study) overlies the Permian sediments, and

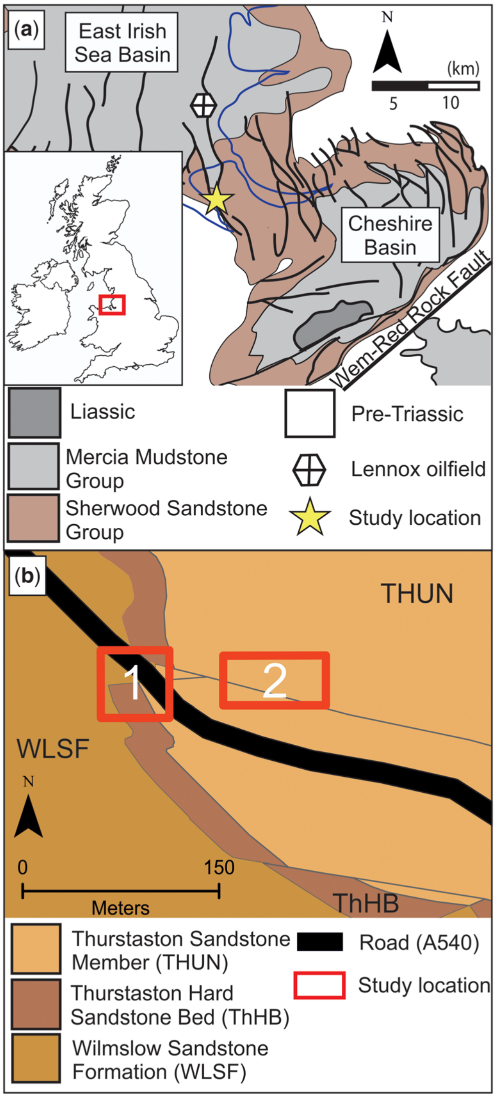

Colour online/colour hardcopy

Fig. 1. (**a**) A simplified geological map of the Cheshire and East Irish Sea basins (edited from Meadows 2006). (**b**) The geology of Thurstaston and the locations used in this study: Telegraph Road (1) and Thurstaston Common (2). Maps adapted from Lexicon of Named Rock Units [XLS geospatial data], Scale 1:50000, Tiles: GB, Version 2011, British Geological Survey, UK. Using: EDINA Geology Digimap Service, http://digimap.edina.ac.uk, downloaded April 2013.

is a 1500 m-thick succession composed of the Cheshire Pebble Beds Formation, the Wilmslow Sandstone Formation and the Helsby Sandstone Formation (Rowe & Burley 1997). The UK migrated from approximately 10° to 30° N of the equator during the Permo-Triassic (Tellam & Barker 2006).

The depositional environment of the Sherwood Sandstone Group in the Cheshire Basin was mixed aeolian and fluvial. The Triassic river systems flowed NW from the Cheshire Basin into the East Irish Sea Basin (Meadows 2006). Post-Triassic successions have been removed across most of the Cheshire Basin following Cretaceous and Tertiary uplift; the youngest deposits (Pre-Quaternary) within the Cheshire Basin are middle Liassic (Rowe & Burley 1997). Meadows (2006) provided a synthesis of existing stratigraphic nomenclature applied to the Early and Middle Triassic Sherwood Sandstone Group in NW England, including East Irish Sea Basin equivalent units based on well correlations that contain various oil and gas discoveries (Knott 1994; Meadows 2006).

Methods

Data were collected from the Cheshire Basin within the Sherwood Sandstone Group at Thurstaston (Fig. 1), on the western side of the Wirral peninsula, 7 km SW of Birkenhead. The presence of deformation bands at Thurstaston has been documented (Knott 1994; Beach *et al.* 1997); however; this paper provides the first detailed analysis of deformation band distribution, as well as a petrographical description and interpretation.

Field data

The outcrop of Lower Triassic Wilmslow Sandstone Formation at Thurstaston (Beach *et al.* 1997), composed of aeolian dune and interdune strata, provides world-class examples of sandstone deformation bands. The Thurstaston Sandstone Member is incorporated within the Wilmslow Sandstone Formation in this study following the most recent pronouncement on the Sherwood Sandstone from the British Geological Society (see Meadows 2006 and references therein). Spatial relationships between Lower Triassic aeolian dune and interdune facies have been well documented within the Cheshire Basin, UK (Mountney & Thompson 2002; Mountney 2012). Two outcrop locations (Fig. 1b) provide a three-dimensional view of the deformation bands:

- Location 1 – Telegraph Road (Figs 2a & 3a), contains conjugate sets of deformation bands within the damage zone of three slip surfaces. The orientation, density and thickness of deformation bands were recorded with proximity to three slip surfaces (over a 5 m linear scanline perpendicular to faulting), within fine-grained (mean grain size of *c.* 170 μm) and overlying coarse-grained sandstone (mean grain size of *c.* 540 μm).
- Location 2 – Thurstaston Common (Figs 2b & 4), allowed for a more extensive study of the relationship between slip surface proximity and deformation band density within coarse-grained sandstone.

Two 30 m linear north–south transects (approximately perpendicular to the strike of the major slip surface) allowed for measurements of fault and deformation band density, spacing and orientation. Using a collection of field photographs covering approximately 1 m^2 of exposure subparallel to bedding, the anastomosing geometry of the deformation bands was captured in detail.

Host-rock grain size and grain-size distribution data were collected using a Beckman Coulter LS13 320 Laser Diffraction Particle Size Analyser (LPSA) for five undeformed coarse- and fine-grained sandstone samples. Owing to the friable nature of both the fine- and coarse-grained sandstones, samples required only gentle disaggregation by hand, and this was analysed under an optical microscope to ensure full disaggregation. As histograms are sensitive to bin selection, sorting was defined by the gradient of cumulative frequency curves (Cheung *et al.* 2012). Grain-size range was calculated by $D_{90}-D_{10}$. D_{90} is the grain size at the upper bound of the 90% fraction, whereas D_{10} is the grain size at the upper bound of the finest 10% fraction. X-ray diffractograms generated from PANalytical X'pert Pro MPD X-ray diffractometer (XRD) quantified mineralogy of both the host rock and the deformation bands within the fine- and coarse-grained sandstones layers.

Microstructural characteristics and petrophysical properties

Orientated samples were sectioned along a north–south plane in order to reveal depositional and diagenetic features, prior to vacuum impregnation with blue epoxy resin to reduce friability and to highlight porosity. A Meiji 9000 optical microscope fitted with an Infinity 1.5 camera with Infinity Analyser software was used to carry out an initial reconnaissance of polished thin sections. Secondary electron images (SE) were collected using a Philips XL30 SEM equipped with an Oxford Instruments Secondary X-ray detector from gold–palladium-coated deformation bands and host rock. Backscattered electron images (BSE) were collected using a Hitachi (TM3000) scanning electron microscope (SEM) and Philips XL30 SEM. Using a Philips XL30 SEM equipped with a K.E. Developments Ltd cathodoluminescence (CL) detector (D308122), SEM-CL images were obtained at 10 kV and spot size 7. SEM-CL images took up to 25 min to collect

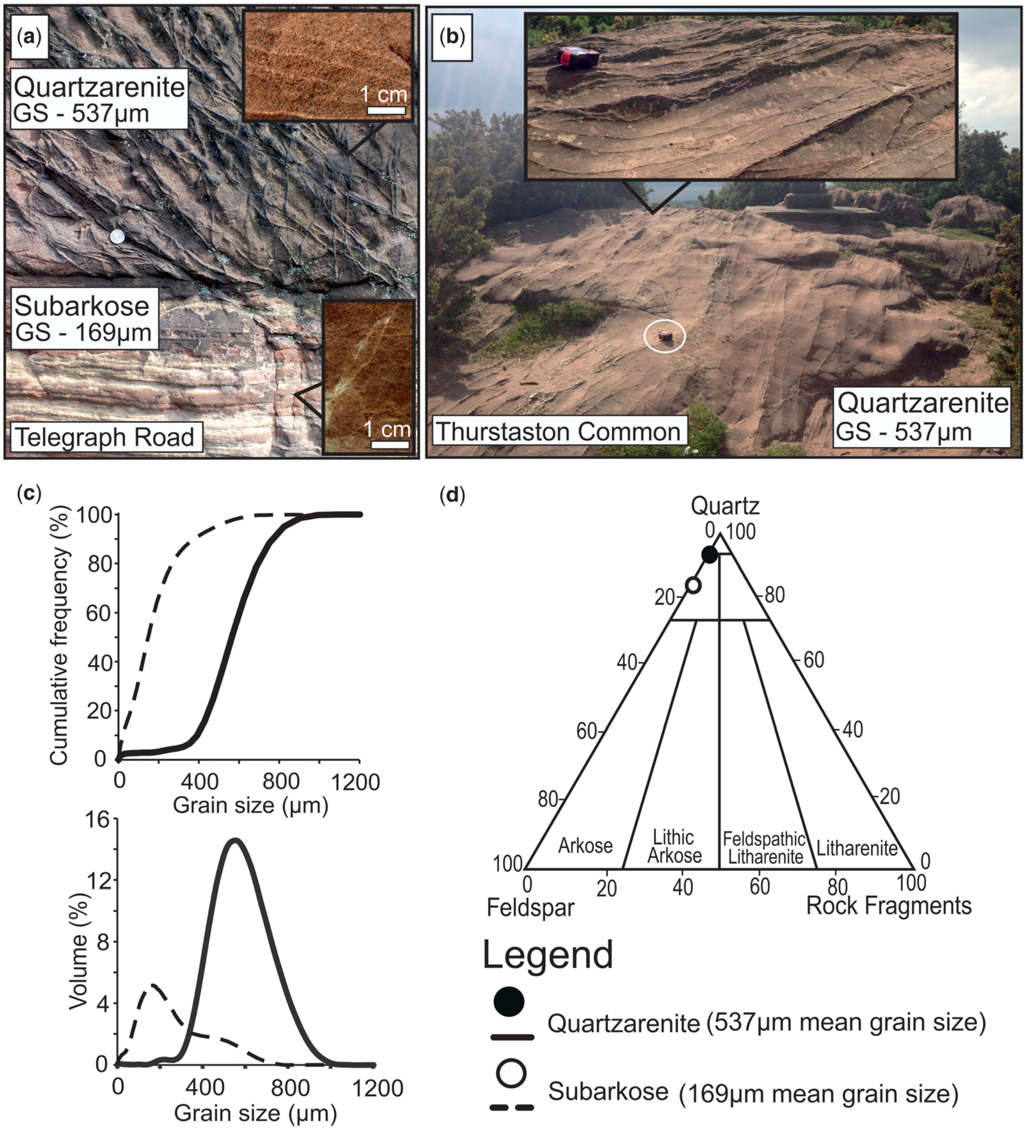

Colour online/ colour hardcopy

Fig. 2. (**a**) Deformation bands confined to the coarse-grained sandstone at Telegraph Road. (**b**) Deformation bands at Thurstaston Common showing a positive relief. (**c**) Grain-size analysis of both the fine- and coarse-grained sandstone at Telegraph Road. (**d**) XRD-determined mineralogy of both the fine- and coarse-grained sandstone at Telegraph Road.

and were gathered by integrating the signal of 16 frames using a slow scanning raster.

Helium porosimetry was used to calculate porosity within the undeformed host rock of both the fine- and coarse-grained sandstone (two core plugs per sandstone). Owing to the friable nature of both sandstones, the core plugs used for the helium porosimetry were not perfectly cylindrical, resulting in a porosity error margin of 4%. Porosity heterogeneity at a deformation band scale (typically <1 mm) cannot be captured on the scale of a core plug (*c.* 25 mm in diameter) and, instead, a petrographical image analysis is typically used (Antonellini *et al.* 1994). It should also be noted that porosity values documented within the literature using helium porosimetry are typically higher than those calculated using digital image analysis (Anselmetti *et al.* 1998; Ogilvie *et al.* 2001). In

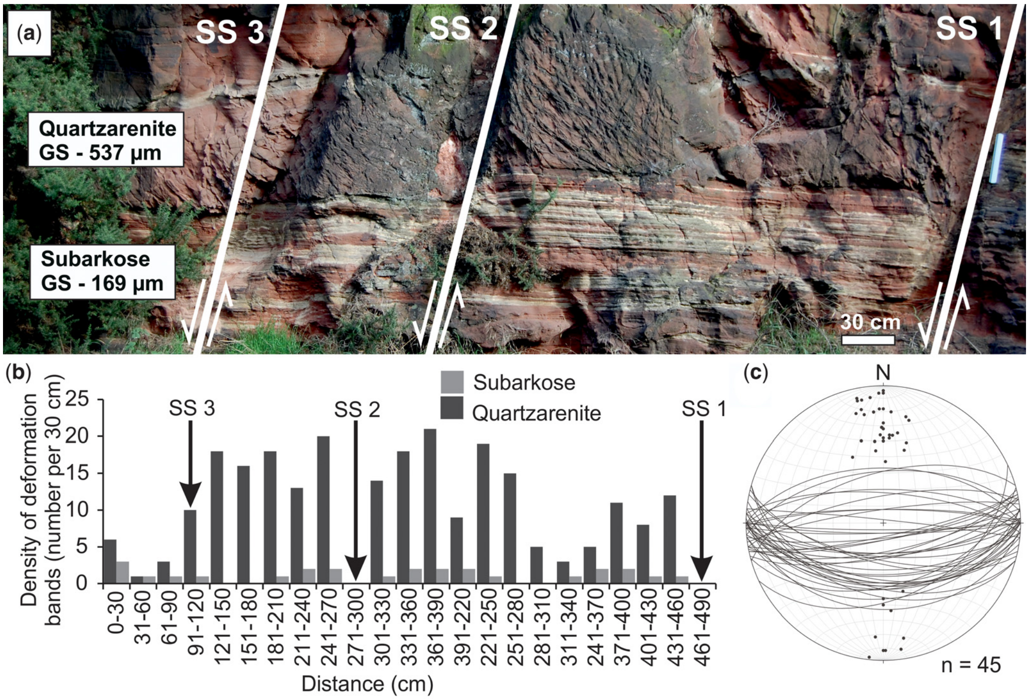

Colour online/ colour hardcopy

Fig. 3. Outcrop at Telegraph Road. (**a**) White lines illustrate the position of the normal faults. The majority of deformation bands end abruptly at the boundary between the overlying coarse-grained quartz arenite and the underlying fine-grained subarkose sandstone. (**b**) Density of deformation bands with proximity to slip surfaces (SS). (**c**) Stereonet representation of the orientation of deformation bands (*n* refers to the number of measurements).

order to calculate porosity within the deformation band and host rock, BSE images (converted to an 8-bit format) have been digitized in ImageJ Analyser (Schneider *et al.* 2012), creating an array of pixels that are assigned a grey-level intensity. Pixel segmentation was then undertaken using a thresholding formula in which black pixels (porosity) and grey pixels (host rock) were differentiated, allowing for the quantification of total optical porosity. Fifteen images (with varying fields of view ranging from *c.* 0.25 to 1.00 mm^2) have been analysed for both fine- and coarse-grained sandstone (i.e. for both the undeformed host rock and deformation band) to ensure accurate results (Ehrlich *et al.* 1991).

Results

Field data

Host-rock properties. Laser particle size analyser and X-ray diffraction data are displayed in Figure 2. Both the coarse-grained sandstone (mean grain size of *c.* 540 μm) and the underlying fine-grained sandstone (mean grain size of *c.* 170 μm) are moderately sorted, with a grain size range of approximately 325 and 340 μm, respectively (Fig. 2c). Minor fining-upward sequences (medium to coarse grained) are present within the overlying cross-stratified foresets of the coarse-grained sandstone (aeolian facies). However, the majority of any pre-existing primary depositional structures are no longer recognizable owing to intense deformation. The underlying fine-grained sandstone (interdune facies) exhibits subhorizontal, centimetre-scale, wavy sandstone laminae with negligible change in grain size both temporally and spatially. X-ray diffraction analysis of the coarse-grained sandstone identified a dominance of quartz (96%), a small quantity of K-feldspar (4–5%) and a trace of illite. X-ray diffraction analysis of the fine-grained sandstone produced a slightly lower percentage of quartz (83%), and an increase in K-feldspar (11%) and illite (6–7%). In all tested samples, there is a negligible difference in the mineralogy (and mineral abundances) of the deformation band and the host rock. The coarse-grained sandstone is classified as a quartz arenite and the fine-grained sandstone is classified as a subarkosic sandstone (Fig. 2d) according the QFR classification (Folk *et al.* 1970).

Fault kinematics and deformation band distribution. The Wilmslow Sandstone Formation (Thurstaston Sandstone Member) at Telegraph Road (Fig. 3a) is faulted by three WNW-trending, high-angle (>80°), north-dipping, normal faults (with respect to bedding), with striations suggesting a minor component of right-oblique slip. Slip surface 1 (SS 1) has an offset of 64 cm, slip surface 2 (SS 2) of 19.5 cm and slip surface 3 (SS 3) of 7 cm: all are subperpendicular to the main NE-trending Formby Point Fault (Fig. 1a) that extends many kilometres northwards, forming a bounding fault to the Lennox oilfield (Yaliz & Chapman 2003). A north- and south-dipping conjugate set (an acute angle of *c.* 55°) of deformation bands display an east–west orientation at both Telegraph Road and Thurstaston Common, parallel to faulting (Figs 3c & 4d). Deformation bands are sporadic within the underlying fine-grained subarkosic sandstone beds and form in swarms within the overlying coarse-grained quartz-arenite sandstone (Fig. 3). Deformation bands are largely confined to the overlying coarse-grained sandstone, and commonly end abruptly at the fine-grained sandstone boundary (Fig. 2a). Deformation bands range from 0.05 mm to 1.2 cm in width, displaying mm-scale offset. The relationship between deformation band density and fault proximity at Telegraph Road is displayed in Figure 3b. Deformation bands broadly increase in density with proximity to the faults. There is no obvious correlation between deformation band density and the magnitude of fault offset.

Slip surfaces observed at Thurstaston Common (Fig. 4) are a continuation of the high-angle WNW-trending faults that can be observed in cross-section at Telegraph Road (Figs 1b & 3). Where slip planes have initiated and offset has occurred, deformation bands tend to localize and orientate in broad zones in proximity to the slip planes. The anastomosing map pattern of the deformation bands (Fig. 4a), as well as the linkage structures (Fig. 4c), can be recognized at the mm- to cm-scale.

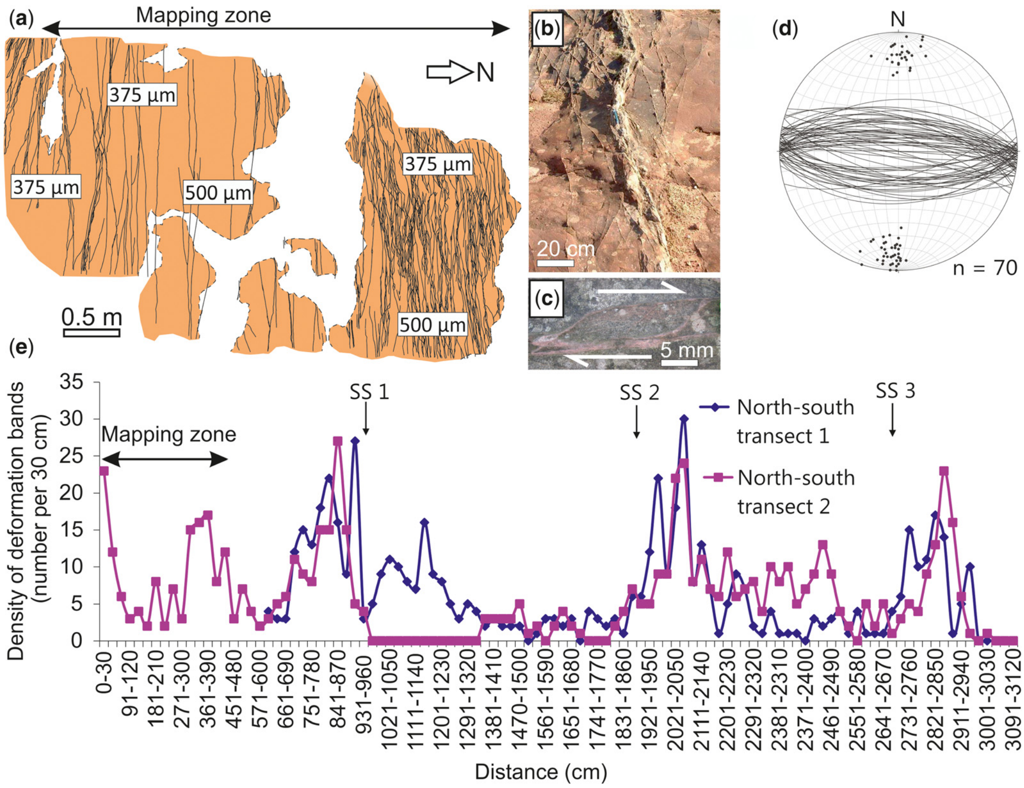

Fig. 4. Outcrop at Thurstaston Common. (**a**) Map of the zones of deformation bands. (**b**) Plan view of deformation bands surrounding a slip surface. (**c**) Linkage structure indicating a strong shear component. (**d**) Stereonet representation of the orientation of deformation bands (*n* refers to the number of measurements). (**e**) Density of deformation bands with proximity to slip surfaces (SS).

Colour online/ colour hardcopy

Microstructures and petrophysical properties

At both study sites (Telegraph Road and Thurstaston Common), deformation bands are classified as cataclastic bands, with the mechanical fracturing of grains being the predominant deformation mechanism. Secondary electron images (Fig. 5a–c) highlight the friable nature of weakly quartz-cemented host-rock grains and intense localized cataclasis, limited to the deformation band core, within the overlying coarse-grained sandstone. Cathodoluminescence images (Fig. 5e) reveal Hertzian grain–grain interaction, with the deformation

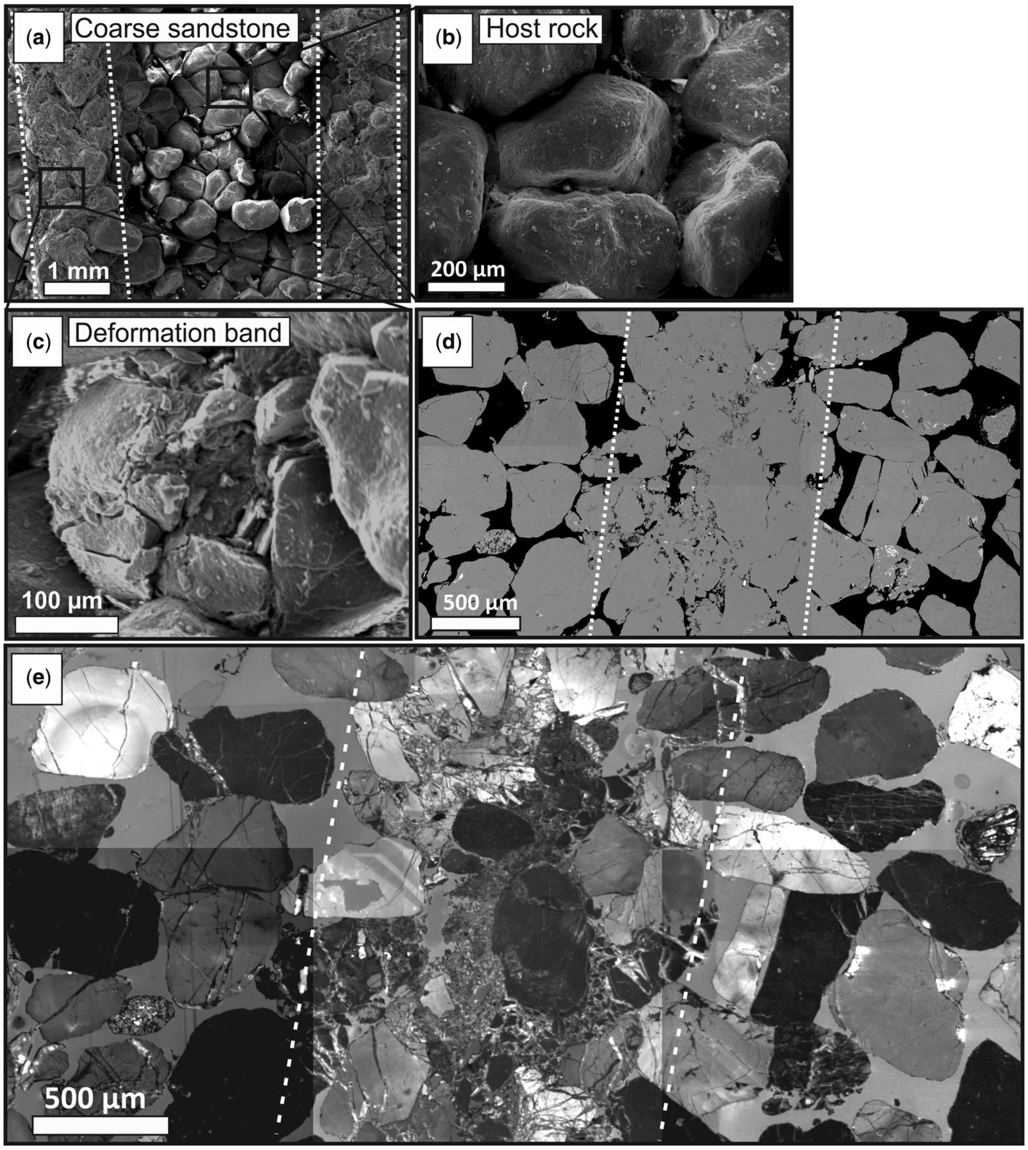

Fig. 5. Deformation bands within the coarse-grained quartzarenite (bandwidth is inferred by the dashed white lines). (**a**)–(**c**) Secondary electron images illustrating the strain localization, poorly cemented host rock and intense cataclasis within the deformation band core. (**d**) BSE image of the deformation band and host rock. (**e**) Collated CL images revealing quartz cementation of the deformation band core and Hertzian fractures.

band core composed of interlocking, fragmented quartz grains cemented by quartz.

The fine-grained host rock is moderately cemented (Fig. 6b), with pore-filling quartz reducing friability; localized comminution of grains produces a deformation band core composed of interlocking detrital clast fragments (Fig. 6c). K-feldspar is preferentially fractured (Fig. 6d–f) within both the deformation band core and the proximal host rock, indicating a strong shear component with a K-feldspar grain being entrained into the deformation band (Fig. 6f). The undeformed host-rock porosity for coarse- and fine-grained sandstone using helium porosimetry is 32 and 15%, respectively. Mean porosity data calculated using image analysis are as follows: the

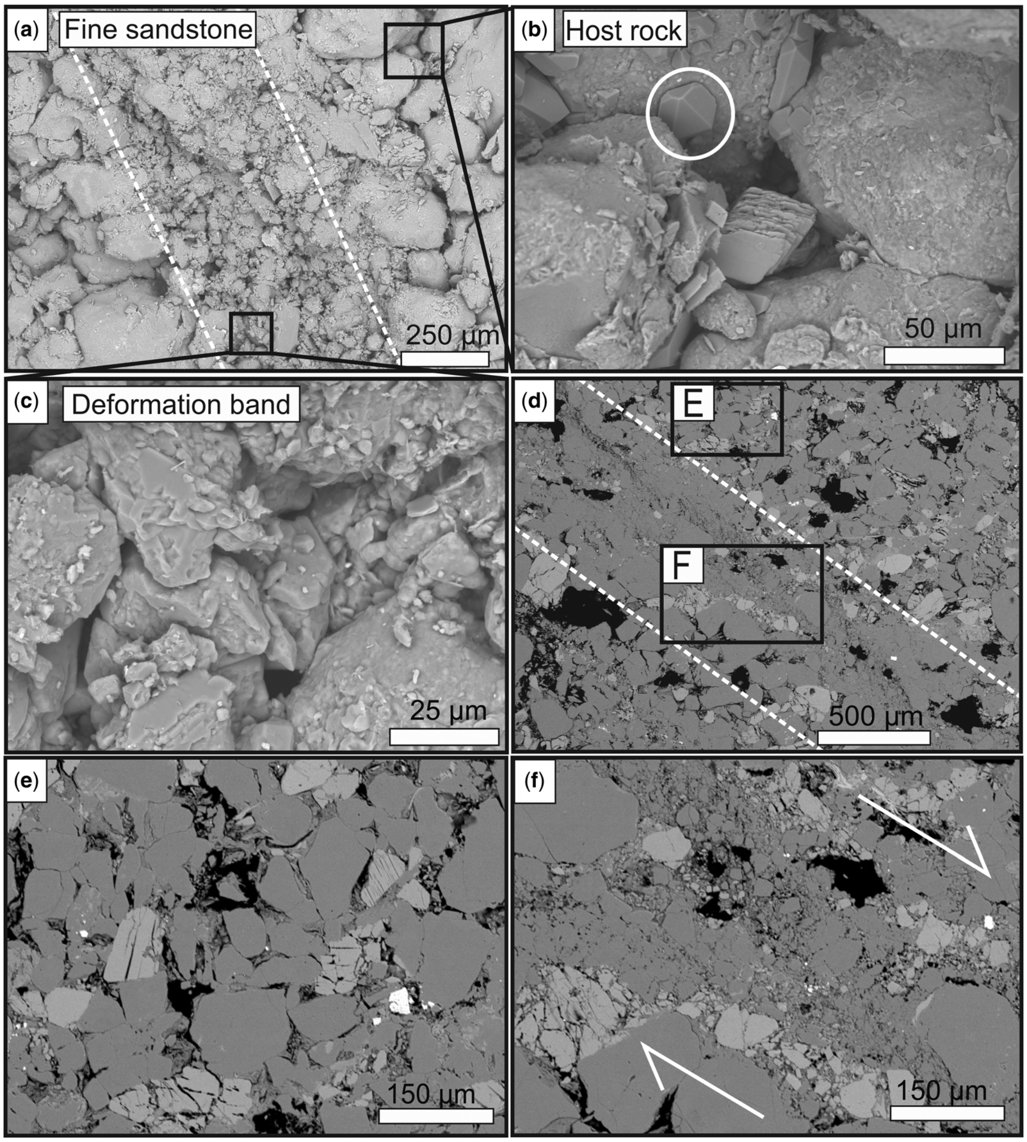

Fig. 6. Deformation bands within the fine-grained subarkosic sandstone (band width is inferred by the dashed white lines). (**a**)–(**c**) Secondary electron images depicting strain localization and grain comminution within the deformation band core, surrounded by a moderately cemented host rock (circled in white). (**d**)–(**f**) BSE images showing preferential fracturing of K-feldspar within the host rock and deformation band core. A strong shear component is indicated by the entrainment of K-feldspar into the deformation band core.

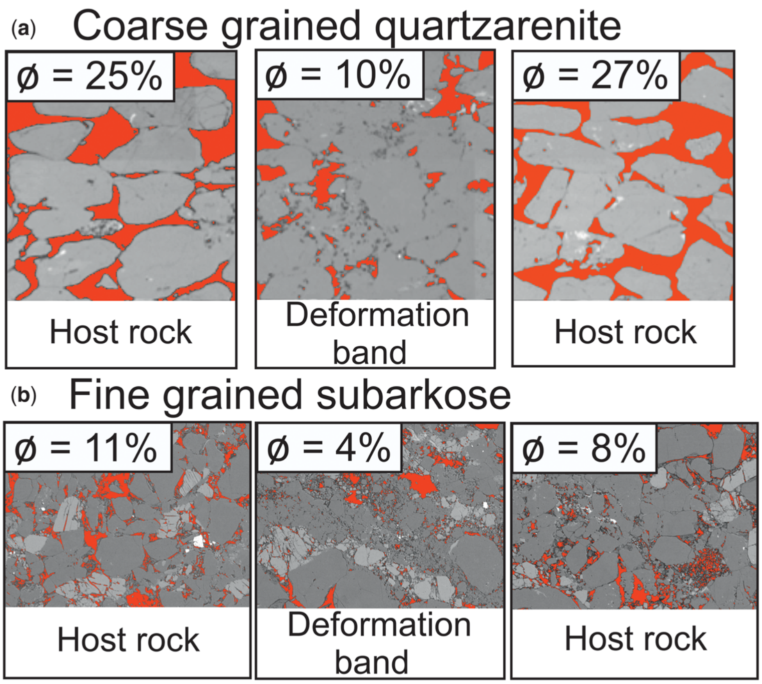

Fig. 7. Porosity calculations using ImageJ analysis software for both the deformation band core and host rock: (**a**) coarse-grained quartzarenite; (**b**) fine-grained subarkosic sandstone.

Colour online/colour hardcopy

undeformed host-rock porosity of coarse-grained sandstone (Fig. 7a) is 26%; porosity has been reduced to 10% within the deformation band core in the coarse sandstones (Fig. 7a); undeformed host-rock porosity for the fine-grained sandstone (Fig. 7b) is 10%; porosity has been reduced to 4% within the deformation band core in the fine sandstones (Fig. 7b).

Discussion

Deformation band distribution and fault proximity

Fault-zone architecture is well documented both in the field and in experimental studies (Antonellini *et al.* 1994; Antonellini & Pollard 1995; Caine *et al.* 1996; Faulkner *et al.* 2010). A typical fault zone comprises of a fault core surrounded by a damage zone (Faulkner *et al.* 2010; Schueller *et al.* 2013). The fault core is an area of localized strain that accommodates the majority of displacement (Faulkner *et al.* 2010; Schueller *et al.* 2013). Damage zones in porous sandstones form by growth of deformation bands prior to the initiation of a slip surface (Schueller *et al.* 2013). Shear strain, state of stress, rock type and microstructural deformation mechanisms are key controls in fault-zone architecture (Ngwenya *et al.* 2003). Hydraulic properties of faults and intrinsic properties of host rocks evolve spatially and temporarily, producing heterogeneous permeability.

At both Telegraph Road and Thurstaston Common, deformation bands broadly increase in density with fault proximity (Figs 3 & 4), consistent with 106 outcrop scanlines recording predominantly cataclastic band density in porous sandstones surrounding extensional faults documented by Schueller *et al.* (2013). Before the initiation of a slip surface, it is evident that deformation band density reaches a maximum of around 20–25 bands per 30 cm section independent of fault displacement, analogous to critical microfracture density recorded within low-porosity granodiorite by Mitchell & Faulkner (2009). The trace of isolated deformation bands in outcrops at Thurstaston Common tend to be straight: however, zones of deformation have an anastomising profile showing linkage structures between neighbouring segments (Antonellini *et al.* 1994), similar to the duplex structure described by Cruikshank *et al.* (1991*a*, *b*). The presence of linkage structures suggests a sense of shear, as they resemble miniature restraining bends (Davis 1999). Deformation band lozenges (defined as the rock volumes between deformation bands) at

Thurstaston Common (Figs 2b & 4b) closely compare to those documented within Goblin Valley, Utah, USA (Awdal *et al.* 2014). Early studies explained the development of closely spaced cataclastic bands (Aydin 1978; Aydin & Johnson 1978) in proximity to low-displacement faults (<10 m throw) by the strain-hardening model, showing an increase in deformation band density with fault displacement (Nicol *et al.* 2013). Cataclastic deformation bands have been suggested to strengthen during formation, thus leading to subsequent band formation within relatively weaker wall rock, adjacent to the earlier-formed bands (Nicol *et al.* 2013). Density counts, the positive relief of deformation bands, linkage structures and microstructural analysis (porosity reduction, interlocking quartz fragments, intense grain comminution increasing grain angularity, shear compaction and preferential quartz cementation) at Thurstaston all support a strain-hardening model, resulting in an increase in deformation band density with fault proximity (Nicol *et al.* 2013). Anomalous results, such as the spike in deformation band density within the mapping zone at Thurstatson Common (Fig. 4e), may be explained by an alteration in host-rock cohesion by neighbouring slip surfaces. Deformation band development explained by a geometric model (see Nicol *et al.* 2013 and references therein) infers that deformation bands are strain weakened and form clusters at geometric complexities or irregularities on faults. Further three-dimensional analysis of the fault geometry and a better understanding of the relative timings of slip-surface formation would be required to apply a geometric model at Thurstaston.

Distribution-localization of deformation bands as a function of intrinsic host-rock properties

Mineralogy. The mineralogy of the host rock is an important controlling factor, with different minerals having varying chemical stability, shape, strength and vulnerability to cleavage fractures (Aydin *et al.* 2006). Mineralogically mature, coarse-grained quartzarenite samples (Fig. 2) display highly localized cataclasis within the deformation band (Fig. 5), with little host-rock fracturing in comparison to the underlying subarkosic sandstone (Fig. 6). In addition to intense cataclasis within the deformation band core, feldspathic subarkosic samples in this study show a higher degree of grain fracturing within the host rock (Fig. 6). Because feldspar fractures at lower differential stress than quartz grains (Rawling & Goodwin 2003), an increase in host-rock deformation may be a result of a selective grain-size reduction of weak grains (Fig. 6e). Preferential feldspar grain-size reduction has also been documented within conjugate sets of deformation bands within poorly consolidated arkosic sands of the Vienna Basin, Austria, by Exner & Tschegg (2012). Intense cataclasis creating angular grains and broadening the grain-size distribution considerably lowers porosity as a result of more efficient grain packing (Main *et al.* 2001; Ogilvie & Glover 2001; Tueckmantel *et al.* 2012).

Porosity, grain size and sorting. Cataclastic deformation bands are common in high-porosity (*c.* 10–35%) sands and sandstones deformed at low confining pressures of <40 MPa at shallow depths of <3 km (Nicol *et al.* 2013). Samples with high porosity have lower rock strength than low-porosity samples as pore spaces coalesce, thus increasing the likelihood of pore collapse and so promoting volumetric reduction deformation (Aydin *et al.* 2006). The critical minimum porosity for deformation band development and propagation is lowered by the addition of shear to compaction (Fossen *et al.* 2011). In order to advance the understanding of fluid migration into subsurface reservoirs, it is important to note that the distribution of porosity (and permeability) in deformed high-porosity sandstones can be markedly anisotropic (Farrell *et al.* 2014). Whilst mapping of a thin section using image analysis yields a more detailed microscale (mm-scale) porosity profile, porosity values may also be dependent upon the scale of the measurement and the thin-section orientation with respect to the orientation of the pores (Ogilvie *et al.* 2001). As expected, helium porosity values are slightly higher than those calculated using image analysis as image analysis does not include microporosity. In addition to mineralogy and porosity, factors such as grain size (Zhang *et al.* 1990; Yin *et al.* 1993; Lothe *et al.* 2002) and sorting (Cheung *et al.* 2012) significantly alter the probability of deformation band development and propagation.

It is well documented that larger grain sizes deform under lower effective stresses than finer-grain material (Zhang *et al.* 1990; Yin *et al.* 1993; Lothe *et al.* 2002; Schultz & Siddharthan 2005; Schultz *et al.* 2010; Tueckmantel *et al.* 2012). Since sandstones at Thurstaston have a similar sorting and fall within the porosity range that allows for deformation band development, it is assumed that host-rock grain size is the principal control on deformation band density. Coarser grains have few contact points, which leads to a larger stress concentration and promotes grain-size reduction (Zhang *et al.* 1990; Yin *et al.* 1993; Lothe *et al.* 2002) in the form of Hertzian grain–grain interaction (Fig. 8a). Hertzian fractures are explained by a complex stress field that is set up when a spherical indenter is pressed onto the surface of an isotropic material. The stresses under and around the indenter contact are compressive; however, outside the

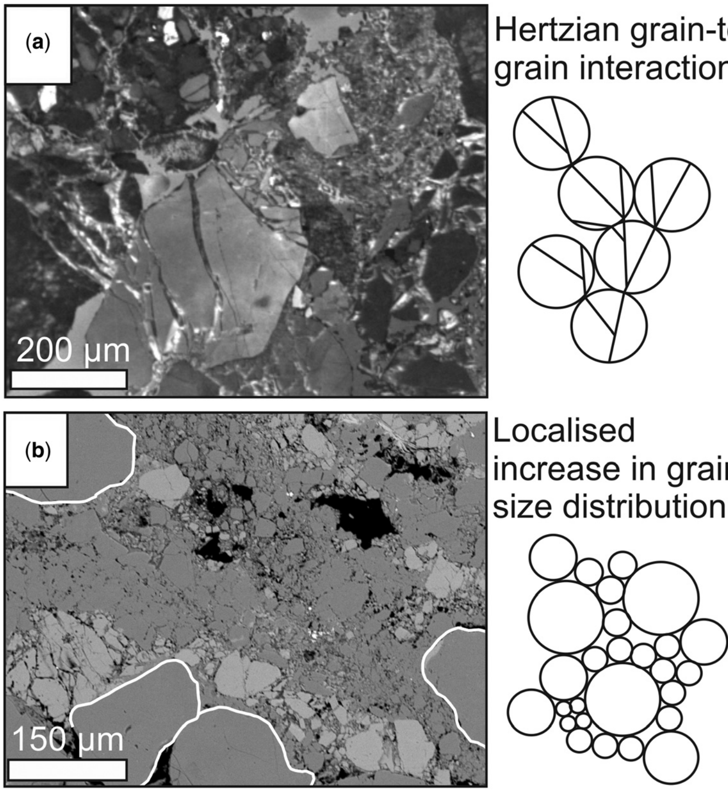

Fig. 8. (**a**) Hertzian grain-contact fracture, creating force chains of fractures propagating into neighbouring grains, promoted by the coarser grain size. The schematic illustration is adapted from Soliva *et al.* (2013). (**b**) Localized increase in grain-size distribution within the fine-grained sandstone, allowing smaller grains to distribute the load over larger particles and so reducing the tensile stress.

contact circle, a radially directed tensile stress is created (Frank & Lawn 1967; Master 2012). Results are consistent with deformation band development within Navajo Sandstone sequences with varying grain size and porosity values at Buckskin Gulsch, Utah, USA (Schultz *et al.* 2010). The corresponding yield envelopes for layers within the Navajo Sandstone are documented to be largest for the fine-grained, less porous sandstones, and smallest for the largest values of porosity and average grain sizes (Schultz *et al.* 2010). The fact that there is a higher density of deformation bands within the overlying coarse-grained sandstone compared to the fine-grained sandstone suggests strain incompatibility between the layers. However, although the density of localized deformation may be different, more strain may have been accommodated through distributed deformation via porosity loss (without fracture) in the finer-grain-sized unit.

In considering mineralogy and grain-size distribution, it is possible to surmise that an increase in K-feldspar content within sandstones will produce a wider grain-size distribution, since K-feldspar has been shown to fracture under lower differential stress than quartz (Rawling & Goodwin 2003; Exner & Tschegg 2012). Thus, a high K-feldspar content may potentially inhibit the development of deformation bands within more feldspathic sandstones, as a non-uniform grain-size distribution allows smaller grains to distribute the load over large particles, and so reduces stress concentrations between grains (Sammis & Ben-Zion 2008; Cheung *et al.* 2012). Petrographical evidence (Fig. 8b) within fine-grained sandstones support the 'constrained comminution' model proposed by Sammis *et al.* (1987), with a localized increase in grain-size distribution within the deformation band core allowing for survivor (or relict) grains.

Implication for sandstone reservoirs

During the appraisal and development of oil and gas fields, analogue studies are helpful for predicting the potential impact on subsurface fluid-flow

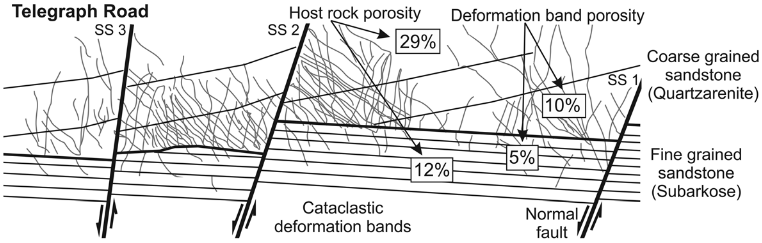

Fig. 9. Schematic synthesis illustration. Deformation bands broadly increase with proximity to faulting. Deformation bands are predominantly restricted to the coarse-grained sandstone. Deformation bands in this study would lower the reservoir quality and potentially compartmentalize the sandstone reservoir.

behaviour. Unfortunately, as the classification and petrophysical measurements of cataclastic deformation bands are not systematic in the literature, it is very difficult to yield a meaningful comparison of results from different study areas (Saillet & Wibberley 2013). However, by combining this study with other analogue studies and experimental datasets, it is likely that reservoir quality predictions will be greatly improved. Cataclastic deformation bands in the literature commonly display lower permeability than the host rock, maximum reductions being of the order of five–six magnitudes and average reductions being around two–three orders (Saillet & Wibberley 2013). Clusters of cataclastic bands have been shown to be as efficient seals as fault cores, withholding up to about a 1 m column of oil and CO_2 (Torabi 2014). The porosity reduction documented in this study would (locally, at least) greatly reduce the reservoir quality, acting as a baffle to fluid flow. For deformation bands to affect well performance, bands must extend over typical well drainage areas: 0.5–1 km^2 for onshore and shallow offshore wells; and 5 km^2 in deep-water wells (Brandenburg *et al.* 2012). Although deformation bands are commonly confined within the damage zones of faults, examples of deformation bands extending over such a large scale have been documented: for example, deformation bands extend approximately 7.5 km^2 at the Valley of Fire, Nevada, USA (Brandenburg *et al.* 2012). In addition to vertical and horizontal continuity and intrinsic host-rock properties, the reservoir-scale impact will also depend on their permeability, orientation, connectivity and abundance (Sternlof *et al.* 2004; Brandenburg *et al.* 2012). The addition of quartz cement, lowering the porosity within the deformation band core, further increases the likelihood of reservoir compartmentalization. Unless accompanied by quartz cement, deformation bands in North Sea reservoirs have not proved to be problematic to oil and gas production (Solum *et al.* 2012). Figure 9 provides a schematic synthesis of the likely distribution of deformation bands and resulting porosity loss associated with conjugate sets of deformation bands within two sandstones with varying intrinsic host-rock properties. If encountered within core, reservoir geologists may use a combination of analogue studies in order to predict the extent of subseismic deformation bands, and the impact on petrophysical properties and reservoir performance. From another point of view, subseismic fault-development mechanisms may be understood by the intrinsic geometry of damage zones connected to the processes of fault growth (Schueller *et al.* 2013).

Specific importance to the East Irish Sea Basin

The Wilmslow Sandstone Formation, part of the Sherwood Sandstone Group, continues north and west into the East Irish Sea Basin, where it is locally known as the St Bees Sandstone Formation (Meadows 2006). The Sherwood Sandstone Group is

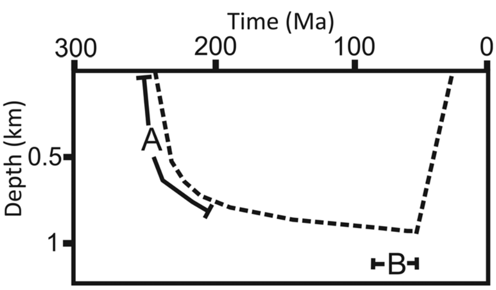

Fig. 10. Schematic illustration of the burial history of the Sherwood Sandstone Group and the timing of deformation band development at Thurstaston. 'A' is the Permo-Triassic rifting forming north–south-trending faults and both the Cheshire and East Irish Sea basins. Development of WNW-trending transfer faults and deformation bands within the Cheshire Basin and, possibly, the East Irish Sea Basin. 'B' is the timing of the underlying Carboniferous source-rock maturation and migration of hydrocarbons into the neighbouring East Irish Sea Basin.

a significant petroleum reservoir within the East Irish Sea Petroleum Province (Duncan *et al.* 1998). A schematic burial history of the outcrop at Thurstaston, including the possible timing of deformation band development (Fig. 10), has been developed based on burial curves constructed by Rowley & White (1998) and the timing of WNW-trending faults suggested by Chadwick (1997). Apatite fission-track analysis from an outcrop 5 km NW of Thurstaston Common seemed to suggest a maximum palaeo-temperature, prior to early Tertiary uplift and cooling, of 90–100°C (Green *et al.* 1997). However, in the undeformed matrix, the high intergranular volume implies limited burial and compaction, and negligible quartz cement (Fig. 6b) implies a maximum temperature much less than 80°C based on depth v. host-rock quartz cement relationships (Worden *et al.* 2000).

Carboniferous source rocks matured during the Late Cretaceous–Early Tertiary, and then oil and gas migrated into the Lower Triassic Sherwood Sandstone (Duncan *et al.* 1998). The timing of the development of WNW-trending faults within both the Cheshire and East Irish Sea basins is poorly constrained. Knott (1994) suggested that WNW-trending faults within the Cheshire Basin formed under a NW–SE-trending maximum horizontal compressive stress regime, present since the Paleocene. It is unlikely that the WNW-trending faults at Thurstaston have formed under a compressive regime, since faults clearly display extensional offsets. Instead, it is possible that these faults, which have formed subperpendicular to, and cross-cut, the main north–south-trending faults are transfer fault (Chadwick 1997). Adding to the complexity, the extensional direction may not have remained constant throughout the evolution of the Cheshire Basin (Chadwick 1997). Despite some uncertainty on the timing of deformation band development within the damage zones of the WNW-trending faults, faulting occurred prior to Tertiary uplift, source-rock maturation and hydrocarbon migration (Fig. 10). Oil and gas migration may have, therefore, been affected by deformation bands in the oil- and gas-bearing offshore equivalent outcrop. As the deformation bands are locally quartz-cemented (thus, further reducing porosity and permeability lower than achieved by simple comminution), careful analysis of cores and borehole image logs for deformation band occurrence and their stratigraphic constraints should be undertaken during field appraisal and the development of oil- and gas-bearing structures in the basin centres.

Conclusions

- Deformation bands in the Triassic sandstone exposed at Thurstaston are cataclastic with a strong component of shear and porosity reduction.
- Deformation bands at Thurstaston broadly increase in density (number/m^2) with proximity to faulting over a scale of several metres.
- Deformation band distribution at Thurstaston is predominantly controlled by grain size. Deformation bands are more abundant within the overlying coarse-grained quartzarenite, and sporadic within the underlying fine-grained subarkose. K-feldspar is preferentially fractured in comparison to quartz grains.
- Deformation bands in Triassic sandstones from Thurstaston have significantly altered the petrophysical properties of the intact rock. Porosity is substantially reduced relative to the matrix due to intense cataclasis and localized quartz cementation. The potential impact of deformation bands in nearby reservoirs in the same lithology could have a detrimental effect on reservoir quality and well performance.

We would like to acknowledge Oliver Hinds for his guidance on statistical grain-size analysis. We are also grateful to John Bedford for assistance during the operation of the helium porosimeter and James Utley for XRD analysis. This manuscript has benefited considerably from the comments of Dr D. Healey and an anonymous reviewer.

References

Anselmetti, F. S., Luthi, S. & Eberli, G. P. 1998. Quantitative characterization of carbonate pore systems by digital image analysis. *American Association of Petroleum Geologists Bulletin*, **82**, 1815–1836.

Antonellini, M. A. & Pollard, D. D. 1995. Distinct element modelling of deformation bands in sandstone. *Journal of Structural Geology*, **17**, 1165–1182.

Antonellini, M. A., Aydin, A. & Pollard, D. D. 1994. Microstructure of deformation bands in porous sandstones at Arches National Park, Utah. *Journal of Structural Geology*, **16**, 941–959.

Awdal, A., Healy, D. & Alsop, G. I. 2014. Geometrical analysis of deformation band lozenges and their scaling relationships to fault lenses. *Journal of Structural Geology*, **66**, 11–23.

Aydin, A. 1978. Small faults formed as deformation bands in sandstone. *Pure and Applied Geophysics*, **116**, 913–930.

Aydin, A. & Johnson, A. M. 1978. Development of faults as zones of deformation bands and as slip surfaces in sandstones. *Pure and Applied Geophysics*, **116**, 931–942.

Aydin, A., Borja, R. I. & Eichhubl, P. 2006. Geological and mathematical framework for failure modes in granular rock. *Journal of Structural Geology*, **28**, 83–98.

Ballas, G., Soliva, R., Sizun, J.-P., Fossen, H., Benedicto, A. & Skurtveit, A. 2013. Shear-enhanced compaction bands formed at shallow burial conditions; implications for fluid flow (Provence, France). *Journal of Structural Geology*, **47**, 3–15.

Baron, M., Parnell, J., Darren, M., Carr, A., Przyjalgowski, M. & Feely, M. 2008. Evolution of hydrocarbon migration style in a fractured reservoir deduced from fluid inclusion data, Clair Field, west of Shetland, UK. *Marine and Petroleum Geology*, **25**, 153–172.

Beach, A., Brown, J. L., Welbon, A. I., McCallum, J. E., Brockbank, P. & Knott, S. 1997. Characteristics of fault zones in sandstones from NW England: application to fault transmissibility. *In*: Meadows, N. S., Trueblood, S. R., Hardman, M. & Cowan, G. (eds) *Petroleum Geology of the Irish Sea and Adjacent Areas*. Geological Society, London, Special Publications, **124**, 315–324, http://doi.org/10.1144/GSL.SP.1997.124.01.19

Caine, J. S., Evans, J. P. & Forster, C. B. 1996. Fault zone architecture and permeability structure. *Geology*, **11**, 1025–1028.

Brandenburg, J. P., Alpak, F. O., Solum, J. G. & Naruk, A. 2012. A kinematic trishear model to predict deformation bands in a fault-propagation fold, East Kaibab monocline, Utah. *American Association of Petroleum Geologists Bulletin*, **96**, 109–132.

Cerveny, K., Davies, R., Fox, G. D. R., Kaufman, P., Knipe, R. & Krantz, R. 2004. Reducing uncertainty with fault-seal analysis. *Oilfield Review*, **16**, 38–51.

Chadwick, R. A. 1997. Fault analysis of the Cheshire Basin, NW England. *In*: Meadows, N. S., Trueblood, S. R., Hardman, M. & Cowan, G. (eds) *Petroleum Geology of the Irish Sea and Adjacent Areas*. Geological Society, London, Special Publications, **124**, 297–313, http://doi.org/10.1144/GSL.SP.1997.124.01.18

Cheung, C. S., Baud, P. & Wong, T. F. 2012. Effect of grain size distribution on the development of compaction localization in porous sandstone. *Geophysical Research Letters*, **39**, L21302.

Cruikshank, K. M., Zhao, G. & Johnson, A. M. 1991*a*. Analysis of minor fractures associated with joints and faulted joints. *Journal of Structural Geology*, **13**, 865–886.

Cruikshank, K. M., Zhao, G. & Johnson, A. M. 1991*b*. Duplex structures connecting fault segments in Entrada sandstone. *Journal of Structural Geology*, **13**, 1185–1196.

Davis, G. H. 1999. *Structural Geology of the Colorado Plateau Region of Southern Utah, with Special Emphasis on Deformation Bands*. Geological Society of America, Special Papers, **342**.

Duncan, W. I., Green, P. F. & Duddy, I. R. 1998. Source Rock burial history and seal effectiveness: key facts to understanding hydrocarbon exploration potential in the East and Central Irish Sea Basins. *American Association of Petroleum Geologists Bulletin*, **82**, 1401–1415.

Ehrlich, R., Crabtree, S. J., Horkowitz, K. O. & Horkowitz, J. P. 1991. Petrography and reservoir physics I: objective classification of reservoir porosity (1). *American Association of Petroleum Geologists Bulletin*, **75**, 1547–1562.

Exner, U. & Tschegg, C. 2012. Preferential cataclastic grain size reduction of feldspar in deformation bands in poorly consolidated arkosic sands. *Journal of Structural Geology*, **43**, 63–72.

Farrell, N. J. C., Healy, D. & Taylor, C. W. 2014. Anisotropy of permeability in faulted porous sandstones. *Journal of Structural Geology*, **63**, 50–67.

Faulkner, D. R., Jackson, C. A. L., Lunn, R. J., Schlische, R. W., Shipton, Z. K., Wibberley, C. A. J. & Withjack, M. O. 2010. A review of recent developments concerning the structure, mechanics and fluid flow properties of fault zones. *Journal of Structural Geology*, **32**, 1557–1575.

Fisher, Q. & Knipe, R. 2001. The permeability of faults within siliciclastic petroleum reservoirs of the North Sea and Norwegian Continental Shelf. *Marine and Petroleum Geology*, **18**, 1063–1081.

Folk, R. L., Andrews, P. B. & Lewis, D. W. 1970. Detrital sedimentary rock classification and nomenclature for use in New Zealand, New Zealand. *Journal of Geology and Geophysics*, **13**, 937–968.

Fossen, H. 2010. Deformation bands formed during soft-sediment deformation: observations from SE Utah. *Marine and Petroleum Geology*, **27**, 215–222.

Fossen, H., Schultz, R. A., Shipton, Z. K. & Mair, K. 2007. Deformation bands in sandstone; a review. *Journal of the Geological Society, London*, **164**, 755–769, http://doi.org/10.1144/0016-76492006-036

Fossen, H., Schultz, R. A. & Torabi, A. 2011. Conditions and implications for compaction band formation in the Navajo Sandstone, Utah. *Journal of Structural Geology*, **33**, 1477–1490.

Frank, F. C. & Lawn, B. R. 1967. On the theory of Hertzian fracture. *Proceedings of the Royal Society of London, Series A. Mathematical and Physical Sciences*, **299**, 291–306.

Green, P. F., Duddy, I. R. & Bray, R. J. 1997. Variation in thermal history styles around the Irish Sea and adjacent areas: implications for hydrocarbon occurrence and tectonic evolution. *In*: Meadows, N. S., Trueblood, S. R., Hardman, M. & Cowan, G. (eds) *Petroleum Geology of the Irish Sea and Adjacent Areas*. Geological Society, London, Special Publications, **124**, 73–93.

Knott, S. D. 1994. Fault zone thickness v. displacement in the Permo-Triassic sandstones of NW England. *Journal of the Geological Society, London*, **151**, 17–25, http://doi.org/10.1144/gsjgs.151.1.0017

Lothe, A. E., Gabrielsen, R. H., Hagen, N. B. & Larsen, B. T. 2002. An experimental study of the texture of deformation bands: effects on the porosity and permeability of sandstones. *Petroleum Geoscience*, **8**, 195–207, http://doi.org/10.1144/petgeo.8.3.195

Main, I., Mair, K., Kwon, O., Elphick, S. & Ngwenya, B. 2001. Experimental constraints on the mechanical and hydraulic properties of deformation bands in porous sandstones; a review. *In*: Holdsworth, R. E., Strachan, R. A., Magloughlin, J. F. & Knipe, R. J. (eds) *The Nature and Tectonic Significance of Fault Zone Weakening*. Geological Society, London, Special Publications, **186**, 43–63, http://doi.org/10.1144/GSL.SP.2001.186.01.04

Master, S. 2012. Hertzian fractures in the sub-dwyka Nooitgedacht striated pavement, and implications for the former thickness of Karoo strata near Kimberley, South Africa. *South African Journal of Geology*, **115**, 561–576.

Meadows, S. N. 2006. The correlation and sequence architecture of the Ormskirk Sandstone Formation in the Triassic Sherwood Sandstone Group of the East Irish Sea Basin, NW England. *Geological Journal*, **41**, 93–122.

Mikkelsen, P. W. & Floodpage, J. B. 1997. The hydrocarbon potential of the Cheshire Basin. *In*: Meadows, N. S., Trueblood, S. R., Hardman, M. & Cowan, G. (eds) *Petroleum Geology of the Irish Sea and Adjacent Areas*. Geological Society, London, Special Publications, **124**, 161–183, http://doi.org/10.1144/GSL.SP.1997.124.01.10

Mitchell, T. M. & Faulkner, D. R. 2009. The nature and origin of off-fault damage surrounding strike-slip fault zones with a wide range of displacements: a field study from the Atacama fault system, northern Chile. *Journal of Structural Geology*, **31**, 802–816.

Mountney, N. P. 2012. A stratigraphic model to account for complexity in aeolian dune and interdune successions. *Sedimentology*, **59**, 964–989.

Mountney, N. P. & Thompson, D. B. 2002. Stratigraphic evolution and preservation of aeolian dune and damp/wet interdune strata: an example from the Triassic Helsby Sandstone Formation, Cheshire Basin, UK. *Sedimentology*, **49**, 805–833.

Ogilvie, S. R. & Glover, P. W. J. 2001. The petrophysical properties of deformation bands in relation to their microstructure. *Earth and Planetary Science Letters*, **193**, 129–142.

Ogilvie, S. R., Orribo, J. M. & Glover, P. W. J. 2001. The influence of deformation bands upon fluid flow using profile permeametry and positron emission tomography. *Geophysical Research Letters*, **28**, 61–64.

Ngwenya, B. T., Kwon, O., Elphick, S. C. & Main, I. G. 2003. Permeability evolution during progressive development of deformation bands in porous sandstones. *Journal of Geophysical Research: Solid Earth*, **108**, 2343.

Nicol, A., Childs, C., Walsh, J. J. & Schafer, K. W. 2013. A geometric model for the formation of deformation band clusters. *Journal of Structural Geology*, **55**, 21–33.

Rawling, G. C. & Goodwin, L. B. 2003. Cataclasis and particulate flow in faulted, poorly lithified sediments. *Journal of Structural Geology*, **25**, 317–331.

Rowe, J. & Burley, S. D. 1997. Faulting and porosity modification in the Sherwood Sandstone at Alderley Edge, northeastern Cheshire: an exhumed example of fault-related diagenesis. *In*: Meadows, N. S., Trueblood, S. R., Hardman, M. & Cowan, G. (eds) *Petroleum Geology of the Irish Sea and Adjacent Areas*. Geological Society, London, Special Publications, **124**, 325–352, http://doi.org/10.1144/GSL.SP.1997.124.01.20

Rowley, E. & White, N. 1998. Inverse modelling of extension and denudation in the East Irish Sea and surrounding areas. *Earth and Planetary Science Letters*, **161**, 57–71.

Saillet, E. & Wibberley, C. A. 2013. Permeability and flow impact of faults and deformation bands in high-porosity sand reservoirs: Southeast Basin, France, analog. *American Association of Petroleum Geologists Bulletin*, **97**, 437–464.

Sammis, C., King, G. & Biegel, R. 1987. The kinematics of gouge deformation. *Pure and Applied Geophysics*, **125**, 777–812.

Sammis, C. G. & Ben-zion, Y. 2008. Mechanics of grain-size reduction in fault zones. *Journal of Geophysical Research*, **113**, B02306.

Schneider, C. A., Rasband, W. S. & Eliceiri, K. W. 2012. NIH Image to ImageJ: 25 years of image analysis. *Nature Methods*, **9**, 671–675.

Schueller, S., Braathen, A., Fossen, H. & Tveranger, J. 2013. Spatial distribution of deformation bands in damage zones of extensional faults in porous sandstones: statistical analysis of field data. *Journal of Structural Geology*, **52**, 148–162.

Schultz, R. A. & Siddharthan, R. 2005. A general framework for the occurrence and faulting of deformation bands in porous granular rocks. *Tectonophysics*, **411**, 1–18.

Schultz, R. A. & Soliva, R. 2012. Propagation energies inferred from deformation bands in sandstone. *International Journal of Fracture*, **176**, 135–149.

Schultz, R. A., Okubo, C. H. & Fossen, H. 2010. Porosity and grain size controls on compaction band formation in Jurassic Navajo Sandstone. *Geophysical Research Letters*, **37**, 1–5.

Soliva, R., Schultz, R. A., Ballas, G., Taboada, A., Wibberley, C., Saillet, E. & Benedicto, A. 2013. A model of strain localization in porous sandstone as a function of tectonic setting, burial and material properties; new insight from Provence (southern France). *Journal of Structural Geology*, **49**, 50–63.

Solum, J. G., Brandenburg, J. P., Naruk, S. J., Kostenk, O. V., Wilkins, S. J. & Schultz, R. A. 2010. Characterization of deformation bands associated with normal and reverse stress states in the Navajo Sandstone, Utah. *American Association of Petroleum Geologists Bulletin*, **94**, 1453–1475.

Solum, J. G., Brandenburg, J. P. & Naruk, S. J. 2012. Characterization of deformation bands associated with normal and reverse stress states in the Navajo Sandstone, Utah: reply. *American Association of Petroleum Geologists Bulletin*, **96**, 877–890.

Sternlof, K. R., Chapin, J. R., Pollard, D. D. & Durlofsky, L. J. 2004. Permeability effects of deformation band arrays in sandstone. *American Association of Petroleum Geologists Bulletin*, **88**, 1315–1329.

Tellam, J. H. & Barker, R. D. 2006. Towards prediction of saturated-zone pollutant movement in groundwaters in fractured permeable-matrix aquifers: the case of the UK Permo-Triassic sandstones. *In*: Barker, R. D. & Tellam, J. H. (eds) *Fluid Flow and Solute Movement in Sandstones: The Onshore UK Permo-Triassic Red Bed Sequence*. Geological Society, London, Special Publications, **263**, 1–48, http://doi.org/10.1144/GSL.SP.2006.263.01.01

Torabi, A. 2014. Cataclastic bands in immature and poorly lithified sandstone, examples from Corsica, France. *Tectonophysics*, **630**, 91–102.

Tueckmantel, C., Fisher, Q. J., Grattoni, C. A. & Aplin, A. C. 2012. Single-and two-phase fluid flow properties of cataclastic fault rocks in porous sandstone. *Marine and Petroleum Geology*, **29**, 129–142.

Ware, P. D. & Turner, J. P. 2002. Sonic velocity analysis of the Tertiary denudation of the Irish Sea Basin. *In*: Doré, A. G., Cartwright, J. A., Stoker, M. S., Turner, J. P. & White, N. (eds) *Exhumation of the North Atlantic Margin: Timing, Mechanisms and Implications for Petroleum Exploration*. Geological Society, London, Special Publications, **196**, 355–370, http://doi.org/10.1144/GSL.SP.2002.196.01.19

Worden, R. H., Mayall, M. & Evans, I. J. 2000. The effect of ductile-lithic sand grains and quartz cement on porosity and permeability in Oligocene and lower Miocene clastics, South China Sea: prediction of reservoir quality. *American Association of Petroleum Geologists Bulletin*, **84**, 345–359.

Yaliz, A. & Chapman, T. 2003. The Lennox Oil and Gas Field, Block 110/15, East Irish Sea. *In*: Gluyas, J. G. & Hichens, H. M. (eds) *United Kingdom Oil and Gas Fields: Commemorative Millennium Volume*. Geological Society, London, Memoirs, **20**, 87–96, http://doi.org/10.1144/GSL.MEM.2003.020.01.07

Yin, H., Marvko, G. & Nur, A. 1993. Grain size effects on porosity, permeability and acoustic velocities in granular materials. *Eos, Transactions of the American Geophysical Union*, **74**, 568.

Zhang, J., Wong, T. F. & Davis, D. M. 1990. Micromechanics of pressure-induced grain crushing in porous rocks. *Journal of Geophysical Research: Solid Earth*, **95**, 341–352.